LANGMUIR Article
Cite This: Langmuir 2019, 35, 8829–8839 pubs.acs.org/Langmuir

Pegylated Metal-Phenolic Networks for Antimicrobial and Antifouling Properties

Hsiao-Tung Zheng,[†] Hoang Linh Bui,[†] Subhendu Chakroborty,[†] Yi Wang,*[,∥,⊥] and Chun-Jen Huang*[,†,‡,§]

[†]Department of Biomedical Sciences and Engineering and [‡]Department of Chemical and Materials Engineering, National Central University, Jhong-Li, Taoyuan 320, Taiwan

[§]R&D Center for Membrane Technology, Chung Yuan Christian University, Chungli, Taoyuan 32023, Taiwan

[∥]School of Ophthalmology & Optometry, Eye Hospital, School of Biomedical Engineering, Wenzhou Medical University, Wenzhou 325035, PR China

[⊥]Wenzhou Institute, University of Chinese Academy of Sciences, Wenzhou 325001, PR China

Supporting Information

Downloaded via BUFFALO STATE on July 21, 2019 at 07:27:35 (UTC).
See https://pubs.acs.org/sharingguidelines for options on how to legitimately share published articles.

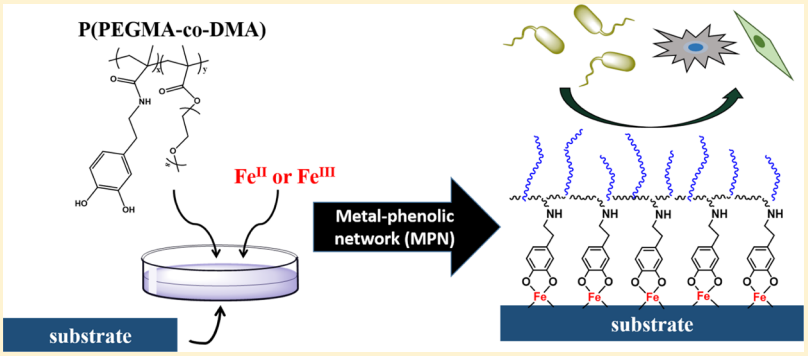

ABSTRACT: Metal-phenolic networks (MPNs) have recently attracted great interest in material chemistry and biomaterials because of their biocompatible, versatile, and multifunctional properties. In this paper, we describe a facile method for preparation of a designable antifouling, antimicrobial, and substrate-independent coating assembled from the coordination of metal ions and catecholic groups. Hydrophilic and catecholic polymers were synthesized by copolymerization of dopamine methacrylamide (DMA) and poly(ethylene glycol)methyl methacrylate (PEGMA) to afford p(PEGMA-*co*-DMA). To investigate the assembly and formation of MPN films, two different metal ions, that is, ferrous (Fe^{II}) and ferric (Fe^{III}) ions, to react with p(PEGMA-*co*-DMA) were compared. The binding constants between iron ions and p(PEGMA-*co*-DMA) have been investigated by ultraviolet−visible spectroscopy (UV−vis). Measurements with atomic force microscopy, contact angle goniometer, and X-ray photoelectron spectroscopy (XPS) were carried out to quantitatively analyze the surface morphology, wettability, and interfacial elemental compositions of coatings, respectively. Moreover, ellipsometric measurements were performed to obtain the film thickness and grafting density. In addition, the pH-responsive property of the MPN films was investigated at different pH values, showing fast disassembly of the networks at low pH. The antifouling properties of the obtained coatings were analyzed by exposing them to bacteria of *Escherichia coli* and *Staphylococcus epidermidis* and NIH-3T3 fibroblasts under observation of fluorescence microscopy and cell imaging analysis. The findings suggest that the MPN from complexation of p(PEGMA-*co*-DMA) and metal ions provides excellent antifouling, pH-responsive, and biocompatible properties on a wide range of substrates. Furthermore, the released iron ions can effectively suppress the growth of bacteria. Accordingly, the new coating architecture offers a universal feature to control surface properties and functionalization for various applications.

INTRODUCTION

The biofouling problem has become a major public health threat worldwide. Unwanted substances, such as proteins, cells, and other biological materials, on the surfaces of medical devices can cause clotting, implant infection, transmission of infectious diseases, and deteriorated functions.[1−6] The aforementioned issues can create financial hardships and potential health risks in the medical and industrial domains.[7,8] Prolonged biofouling on biomaterial devices may lead to the development of the notorious biofilm, in which microorganisms enhance the viability, improve adaptation to the change of their micro-environment, and tolerate many biocidal approaches.[9,10] To

Received: April 24, 2019
Revised: June 5, 2019
Published: June 9, 2019

© 2019 American Chemical Society

DOI: 10.1021/acs.langmuir.9b01196
Langmuir 2019, 35, 8829−8839

address the emerging problem, recent studies demonstrate two major strategies: surface protection from attachment and degradation of biofoulants.[11] One of the most intensively studied antifouling materials is poly(ethylene glycol) (PEG), a water-soluble polymer with low toxicity and high steric repulsion for frequent use in medical and industrial applications.[12−17] However, implementation of the PEG-derived coating materials is limited by the design of attachment groups to lead to a constraint on the specific substrates.[18−21]

Dopamine (DA), a catechol-containing molecule, has moved into the limelight as a novel building block for developing substrate-independent coating materials for a myriad of applications, such as functional adlayers for post-conjugation, antimicrobial and antifouling properties, anticorrosion treatments for microtribology, and enhancement of osteointegration.[22−24] DA coatings were inspired by mussels adhesive proteins (MAPs) secreted by marine mussels, containing a high amount of 3,4-dihydroxy-L-phenylalanine and lysine amino acids.[24] The Waite group found that Fe^{III} participates in the in vivo coordination cross-linking of the MAPs.[25,26] The concentration of Fe^{III} correlates with the mechanical properties, which is supposed to be caused because of strong, yet pH reversibly breakable catechol−Fe^{III} bonds. Very recently, metal-phenolic networks (MPNs), the supramolecular coordination structures comprising metal ions and polyphenols, are found to be useful for preparation of multifunctional hydrogels and surface modification.[27−29] The complexation between metal ions and polyphenols occurs through a coordination reaction from a ligand that donates a nonbonding electron pair to the empty orbitals in a transition metal ion.[30] The Caruso group reported a simple and rapid assembly of metal phenolic gels (or metallogels) by the direct gelation of natural tannic acid (TA) and group (IV) metal ions, such as Ti^{IV}.[28,31] The large number of gallol groups on TA facilitates efficient coordination-driven cross-linking, leading to three-dimensional stable MPNs. The metallogels exhibit pH-modulated mechanical property, shape persistence, adhesiveness, self-healing, and capability of co-gelation with various metal ions, nanomaterials, and polymers.[32] Moreover, the conformal coatings based on complexation of catechol/gallol−metal ions were developed on different substrates with various geometries, such as planar surfaces and nanomaterials, by simply mixing in one pot.[28] MPNs are widely applied to the fields of bioimaging, drug delivery, and biotechnology through a novel green route to fabricating advanced materials.[33−35]

Synthetic catechols offer large versatility in material designs. To prevent nonspecific adsorption, PEG-based catecholic materials were developed for the formation of MPNs and antifouling coatings. Holten-Andersen et al. reported a self-healing hydrogel based on the coordination of a 4-arm-poly(ethylene glycol) (4-arm-PEG)−catechol and Fe^{III}.[36] Ju et al. developed PEG−polyphenol, synthesized by conjugating catechol groups onto each terminus of an eight-arm-PEG.[37] PEG−MPNs were assembled on $CaCO_3$ particles by adding Fe^{III} into a PEG−polyphenol solution, followed by increasing the pH to form metal-phenolic coordination complexes. PEG−MPN capsules exhibit significantly higher resistance to nonspecific protein adsorption and cellular association, and pH-degradability, which allows the controlled release of cargo for potential intracellular drug delivery. Kang et al. synthesized six-arm PEG catechol and deposited multilayered PEG films on various polydopamine-premodified surfaces through catechol−Fe^{3+}−catechol interactions for strong resistance against marine diatom adhesion.[38] However, the catecholic building block prepared from the conventional polymerization has not been found.

In this work, for facile preparation and good versatility of a phenolic building block for the formation of MPNs, mussel-inspired DA methacryl amide (DMA) and poly(ethylene glycol)methacrylate (PEGMA) were co-polymerized to afford p(PEGMA-*co*-DMA) for formation of antifouling and antimicrobial coatings on various types of substrates. The binding affinities of Fe^{II} and Fe^{III} ions with p(PEGMA-*co*-DMA) were determined by UV−vis photospectroscopy. The MPN films were prepared by simply mixing p(PEGMA-*co*-DMA) and iron ions simultaneously.[27,39] The thickness, grafting density, and distance between grafting sites of p(PEGMA-*co*-DMA)/Fe MPNs were well controlled by deposition cycle numbers. X-ray photoelectron spectroscopy (XPS), contact angle, and atomic force microscopy (AFM) were applied to characterize the interfacial chemical composition, wettability, and morphology of the films. The antifouling properties of p(PEGMA-*co*-DMA)/Fe MPNs were accessed by attachment tests of mammalian cells and bacteria under observation of microscopy. The fouling resistance of the p(PEGMA-*co*-DMA)/Fe MPNs can be achieved on various types of substrates, glass (SiO_2), nitinol alloy, polydimethylsiloxane (PDMS), polystyrene (PS), wafer, and TiO_2. Moreover, we observed the antimicrobial capability of the p(PEGMA-*co*-DMA)/Fe MPNs, likely because of protein dysfunction, oxidative stress, or membrane damage by metal ions.[40] The MPN coatings offer unique features, such as facile preparation, substrate-independent deposition, and effective antifouling and antimicrobial properties. The MPN building blocks, including polymers and metal ions, can be assembled onto different materials with various geometric structures to display their functionalities. More importantly, DMA can be incorporated with a wide variety of monomers via conventional vinyl polymerization for preparation of functional building blocks of MPNs. Therefore, we believe that the ingenious approach offers a step toward addressing the biofouling problem on the surface of medical devices.

EXPERIMENTAL SECTION

Materials. DA hydrochloride, methacrylic anhydride, tetrahydrofuran (THF), ethyl acetate, sodium sulfate anhydrous, hexane 4,4-azobis(4-cyanovaleric acid) (ACVA), poly(ethylene glycol)methyl ether methacrylate (PEGMA) (M_w = 475 Da), Trizma hydrochloride solution, acetone, ethanol, phosphate buffered saline (PBS), iron(II) chloride, iron(III) hexahydrate, and dimethyl sulfoxide were purchased from Sigma-Aldrich, U.S.A. Sodium hydroxide (NaOH), hydrochloric acid (HCl), MTT assay kit, sodium dodecyl sulfate (SDS), LIVE BacLight Bacterial Viability kit, and Dulbecco's Modified Eagle's medium (DMEM) were obtained from Thermo Scientific, U.S.A. Sodium tetraborate was acquired from Showa, Japan. Sodium bicarbonate was acquired from Acros Organics, Belgium. PDMS was prepared using SYLGARD 184 Silicone Elastomer Kit from Dow Corning, U.S.A. Difco LB Broth, Miller (Luria−Bertani) was purchased from BD Biosciences, U.S.A. *Escherichia Coli* and *Staphylococcus epidermidis* were provided by Bioresource Collection and Research Center of Taiwan. NIH-3T3 fibroblasts were provided by Food Industry Research and Development Institute, Taiwan. Fetal bovine serum (FBS) and tissue culture PS were purchased from Gibco, U.S.A.

Synthesis of DMA. Synthesis of DMA was referred to a previous work[41] with minor modification. Tetraborate (10 g) and 4 g of sodium bicarbonate were dissolved in 100 mL of deionized (DI) water. The solution was degassed with nitrogen for 20 min, followed by the addition of 5 g of DA hydrochloride powder into the above alkaline solution. Methacrylic anhydride (4.7 mL) in 25 mL of THF was

DOI: 10.1021/acs.langmuir.9b01196
Langmuir 2019, 35, 8829−8839

Scheme 1. Preparation of DMA Monomer and PEGMA-*co*-DMA Copolymer

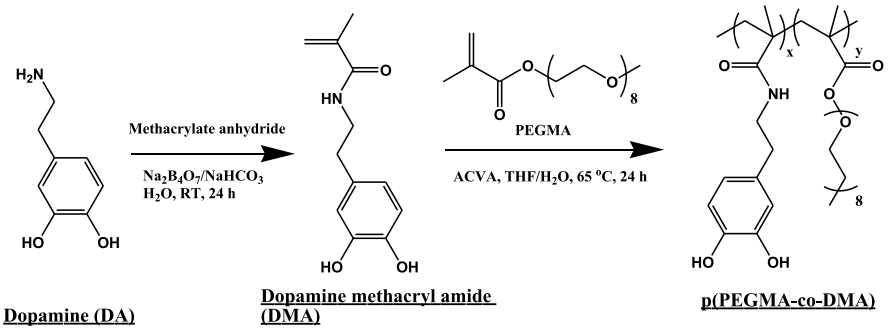

Table 1. Characterization of p(PEGMA-*co*-DMA) Polymers Using NMR and GPC

	feed ratio[a]	actual ratio[b]	theoretical M_n[c] (Da)	exp. M_n[d] (Da)	PDI[d,e]	DP[d,f]
p(PEGMA$_7$-*co*-DMA$_3$)	7:3	7.1:2.9	19 945	15 797	1.07	39
p(PEGMA$_8$-*co*-DMA$_2$)	8:2	7.9:2.1	21 213	15 894	1.02	37
p(PEGMA$_9$-*co*-DMA$_1$)	9:1	8.8:1.2	22 481	16 218	1.03	36

[a]Feed mole ratios of PEGMA/DMA. [b]Determined by ^{1}H NMR spectrum and the integrated area ratio of methylene protons adjacent to ester group of PEGMA and aromatic protons of DMA in polymer chains. [c]M_n = number-averaged molecular weight. [d]Determined by GPC. [e]PDI = M_w/M_n. M_w = weight-averaged molecular weight. [f]DP = M_n/M_0. M_0 = molecular weight of the monomer unit.

prepared separately and added slowly to the DA-containing solution. 1 M NaOH was added dropwise into the reaction flask to achieve moderately basic mixture (pH 8 or above). The reaction mixture was protected in nitrogen and then stirred for 24 h. Afterward, the resulting solution was filtered. To the aqueous solution was added 50 mL of ethyl acetate and acidified with 6 M HCl to pH 2. The organic layer was isolated from the acidified solution after 1 min of phase separation, and dried by adding anhydrous $MgSO_4$. Then, the solution was concentrated with a rotary evaporator. A precipitated solid was formed in the concentrated solution by stirring vigorously with hexane. The white powder was acquired by centrifuging the solution at 9000 rpm for 10 min and rinsed three times by dissolving in 20 mL of ethyl acetate and precipitating with 300 mL of hexane to improve product purity. The synthesis process is shown in Scheme 1. The product was dried in vacuum for 6 h and achieved production yield of 85%. ^{1}H NMR (500 MHz, DMSO-*d*, δ) in Figure S1: 7.93 (NH, 1H), 6.61 (Ph, 2H), 6.44 (Ph, 1H), 5.59 (CH_2−C, 1H), 5.23 (CH_2−C, 1H), 3.23 (NH−CH_2−, 2H), 2.55 (CH_2−Ph, 2H), and 1.84 (CH_3, 3H). ESI-MS: m/z 222.3 (M + H^+).

Preparation of p(PEGMA-*co*-DMA) Copolymer. The copolymer was prepared using random copolymerization of PEGMA and DMA as reported in the literature as shown in Scheme 1.[41] In detail, different molar ratios of DMA and PEGMA (Table 1) were dissolved in 15 mL of THF and 15 mL of DI water, respectively. ACVA (0.2 mmol) was added to the mixture of DMA and PEGMA as thermal initiator. The mixture was then purged with nitrogen for 30 min. The copolymerization proceeded at 65 °C for 24 h. After the reaction, the product was concentrated to a volume of 2 mL using a rotary evaporator, and the unreacted monomers were then dialyzed against DI water for 24 h using a dialysis membrane with molecular weight cut-off of 3500 Da. The final solution in the dialysis membrane was concentrated under reduced pressure to obtain a yellow oil of the p(PEGMA-*co*-DMA) copolymer.

Formation of MPN on Substrates. The MPN deposition technique followed the previous study.[29] Substrates (1 × 2 cm in size), that is glass (SiO_2), silicon wafer, TiO_2, nitinol (Ni−Ti) alloy (Jp&J Technic), were washed with 1% SDS to remove surface contamination, then rinsed in DI water and ethanol 95% for 10 min of each step under sonication. The substrates were eventually treated with oxygen plasma (PDC-32G, Harrick Plasma) for 10 min. PDMS and PS were used as they were received. One-pot deposition was employed for the MPN formation. For preparation of the MPN solution, p(PEGMA-*co*-DMA) (10 mg mL^{-1}) and $FeCl_2{\cdot}4H_2O$ or $FeCl_3{\cdot}6H_2O$ (1 mg mL^{-1}) were added to 10 mM Tris buffer at pH 8.5. Then, the substrates were soaked in the solution, and shaken at 50 rpm at room temperature. After 18 h, the substrates were rinsed with DI water for 30 s and then dried with the nitrogen stream. The coating process can be repeated for several cycles. Herein, the samples prepared by a single deposition number were denoted as "1-Fe^n", where "n" is the valence of the iron ion and "1" indicates the deposition number. The samples prepared by two deposition numbers were denoted as "2-Fe^n", and the like. After each cycle, substrates were rinsed with DI water and dried with the nitrogen stream. For the control sample, p(PEGMA-*co*-DMA) alone in the Tris buffer at pH 8.5 without the metal ion was prepared for the deposition of the thin films. After the coating process, substrates were rinsed with DI water and dried with a nitrogen stream.

Characterizations for p(PEGMA-*co*-DMA). Characterization with gel permeation chromatography (GPC) equipped with a Viscotek RI detector (VE3580, Malvern) was obtained using DI water as the mobile phase, and polyethylene oxide (PEO) (M_w 450−45 000) as a calibration standard. The experiment was conducted at a flow rate of 1 mL min^{-1} at 40 °C using a A3000-Single-pore GPC/SEC column (300 × 8 mm) and CLM3023-AGuard column (50 × 6 mm). The samples were filtered by 0.45 μm filters before analysis.

UV−Vis Spectroscopic Analysis. The equilibrium constant between p(PEGMA-*co*-DMA) and the metal ion was calculated based on previous work.[42] A UV−vis spectrophotometer (model V-600, Jasco) was used in a scan range from 200 to 750 nm for the evaluation of the interaction between catechol moieties and metal ions. p(PEGMA-*co*-DMA) was added to Tris buffer (pH 8.5) to yield the concentration of 0.1% w/v. The Fe solution was first prepared at a concentration of 20 mM by dissolving in oxygen-free DI water. Then, the solution was mixed with the p(PEGMA-*co*-DMA) solution to attain a series of metal ion concentrations from 10 to 100 μM. After adding metal ions, the final concentration of copolymers was adjusted to 0.001% w/v and maintained throughout the experiments. The reaction was preceded at room temperature for 10 min before assessment.

The interaction between phenolic compound can be demonstrated by the following reaction

$$\text{Phenolic compound} + \text{metal ion} \leftrightarrow \text{phenolic compound:metal ion}$$

The equilibrium binding constant k in M^{-1} between copolymers and metal ions was defined by eq 1

$$k = \frac{[\text{phenolic compound:metal ion}]}{[\text{phenolic compound}][\text{metal ion}]} \quad (1)$$

DOI: 10.1021/acs.langmuir.9b01196
Langmuir 2019, 35, 8829−8839

According to the reference,[42] data from UV−vis can be interpreted as a plot of $1/(A - A_o)$ versus $1/L$ by eq 2

$$\frac{1}{A - A_o} = \frac{1}{\varepsilon \cdot n \cdot a \cdot k}\frac{1}{L} + \frac{1}{\varepsilon \cdot n \cdot a} \quad (2)$$

where A and A_o are the absorbances of metal ion−copolymer complex and copolymer alone, respectively, and ε is the extinction coefficient of catechol moiety, n is the number of metal-binding sites, a is the concentration of copolymers, and L is the concentration of metal ions.[42]

From eq 2, the graphs show a linear relationship for all of the metal ions. The binding constants, k, were calculated as the ratio of the intercept on the vertical axis to the slope, leading to eq 3.

$$k = \frac{1}{\varepsilon \cdot n \cdot a}\frac{1}{\text{slope}} = \frac{\text{intercept on}\frac{1}{A - A_o}\text{axis}}{\text{slope}} \quad (3)$$

AFM Imaging for MPN Coatings. To investigate the surface morphology of MPN coatings AFM (SPA-400, Seiko) was employed. In this work, the tapping mode (NanoWorld innovative technologies) was applied with aluminum-coated silicon cantilevers (Tap300Al-G, Budget sensors with a force coefficient of 40 N m^{-1} and resonant frequency of 300 kHz) at a scanning speed of 1 Hz and scanning range of 5 × 5 μm^2.

XPS Characterization. The elemental composition of the MPN coatings on substrates was revealed in XPS. The spectra were determined using a PHI 5000 VersaProbe (ULVAC-PHI, Chigasaki, Japan) system, including a microfocused Al X-ray beam (100 μm, 25 W) at a photoelectron take-off angle of 45° in an ultrahigh vacuum of 2 × 10^{-8} Pa and a dual-beam charge neutralizer (7 V Ar^+ and flooding 30 V electron beam) employed to compensate for the charging effect. The photoelectron spectra were acquired with pass energy set to 58.7 eV. Glass (SiO_2) was chosen as the substrate for assessment. The spectra were recorded from C 1s, N 1s, O 1s, Si 2p, and Fe 2p for further analysis. The recorded binding energies (BEs) were corrected according to the glass (SiO_2) signal peak position of 103.5 eV.

Contact Angle Measurement. The contact angle at the solid−liquid interface was measured using a contact angle goniometry (Phoenix Mini, Phoenix). The microsyringe produces droplets of 5 μL, and each sample was measured in triplicate.

Ellipsometric Measurement. The thickness of MPN coatings was determined at room temperature using an ellipsometer (alpha-SE, J.A. Woollam Co., Inc.) with He−Ne laser (λ = 632.8 nm) at a fixed incident angle of 70°. The refractive index of the coating on the substrate was fixed at n = 1.46. The bare substrates were measured to find the Ns (2.5), Ks (−3.2), and refractive index (n = 1.00) of the ambient. The thickness of the coating was automatically calculated using the Cauchy model, and measured at least three times at random positions. Grafting density and distance between grafting sites were calculated according to eqs 4 and 5

$$\Sigma = \Gamma \times N_A \times \frac{10^{-21}}{M_n} = \frac{6.03\Gamma \times 100}{M_n} = \frac{6.03 \times h \times \rho \times 100}{M_n} \quad (4)$$

and

$$D = \left(\frac{4}{\pi\Sigma}\right)^{1/2} \quad (5)$$

where Σ is the graft density (chain nm^{-2}), D is the distance between grafting sites (nm), Γ is the copolymer surface coverage (mg m^{-2}), N_A is Avogadro's number, h is the thickness of the copolymer layer (nm), ρ is the density of the copolymer, which is assumed to be 1 g cm^{-3} and M_n is the number-averaged molecular weight of grafted copolymers.[43,44]

Cytotoxicity Tests. The cell viability of copolymers was evaluated by an MTT test with NIH-3T3 fibroblasts. In detail, cells in DMEM containing 10% FBS were seeded in a 96-well plate to get 6 × 10^3 cells per well, and incubated at 37 °C and an atmosphere content of 5% CO_2 for 16 h. The culture medium was then removed. Serum-free DMEM containing p(PEGMA-*co*-DMA) copolymers (200 μL) at different concentrations was added to the well, and incubated for 24 h. The MTT solution, prepared at a concentration of 50 mg mL^{-1} in PBS, was then added to a 96-well plate and incubated for another 3 h. After removing the MTT solution, 20 μL of DMSO was added to dissolve the purple crystal of formazan. The Synergy HT Multi-Detection Reader (BioTek Instruments, Winooski, VT) was used to determine the absorbance at 540 nm. The control experiment was carried out with the cells in the absence of the polymer. The reported value is the mean from three replicates and is expressed as a percentage with respect to the values from the control samples.

Antimicrobial Test. Two bacterial strains, *E. coli* and *S. epidermidis*, were chosen as representatives of Gram-negative and Gram-positive bacteria, respectively. In this work, bacteria were incubated in 25 mL of LB medium at 37 °C and 5% CO_2 by shaking at 200 rpm for 16 h. Bacteria were harvested by centrifuging at 4000 rpm for 5 min, followed by washing with PBS three times under the same centrifugation setting. Finally, the bacterial concentration was diluted with sterile PBS to an optical density at 670 (OD_{670}) of 0.1, which corresponds to a concentration of 8 × 10^7 cells mL^{-1}. The bacterial solution was used for subsequent bacterial-fouling tests.

MPN-coated substrates were placed in a 12-well plate. The bacterial solution in PBS (2 mL) was added to each well, and incubated at 37 °C and 5% CO_2 for 3 h. After that, substrates were washed with sterile PBS by shaking at 100 rpm for 5 min three times to remove nonadherent bacteria. LIVE/DEAD BacLight was used to stain bacteria in a dark room at room temperature for 15 min. Then, the substrates were shaken with PBS at 100 rpm for 5 min and imaged using a fluorescence microscope (Zeiss Microscope Axio Observer A1, Germany) with a magnification of 20× and excitation wavelength at 488 nm. The live bacteria emitted green light at wavelengths between 510 and 540 nm; the dead bacteria emitted red light at wavelengths between 620 and 650 nm. In each sample, five locations were randomly selected, and quantitative analysis of bacterial adhesion was performed using ImageJ software (developed at National Institutes of Health, MA).

Cell Adhesion Tests. Mouse NIH-3T3 fibroblasts were used for the cell adhesion assay. The cell solution was diluted with DMEM containing 1% FBS to achieve 1 × 10^5 counts mL^{-1}. The MPN-modified substrates were immersed in 75% ethanol for 30 s for sterilization, then washed three times with sterilized PBS. The substrates were then soaked with culture media in a 24-well plate at 37 °C, 5% CO_2 for 30 h. After that, the substrates were washed with sterile PBS by shaking at 50 rpm at room temperature for 10 min, followed by imaging under an optical microscope at a magnification of 20× for assessment. The number of cells and the cell coverage area was calculated using ImageJ software.

RESULTS AND DISCUSSION

The biomimetic catecholic polymers were obtained by copolymerization of PEGMA and DMA with the feed molar ratios of 7:3, 8:2, and 9:1 to afford p(PEGMA-*co*-DMA). The products were denoted as p($PEGMA_7$-*co*-DMA_3), p($PEGMA_8$-*co*-DMA_2), and p($PEGMA_9$-*co*-DMA_1), respectively, corresponding to their feed mole ratios. The actual compositions, molecular weight, polydispersity index (PDI), and degree of polymerization (DP) were analyzed by ^{1}H NMR spectroscopy and GPC, as shown in Table 1. Generally, the actual molecular compositions of the products from the synthesis were in agreement with the monomer feed mole ratios. The mole ratios of catecholic DMA in polymer chains varied from 10 to 30%. The number-averaged molecular weight (M_n) of three polymers were controlled to a narrow range of around 15 000 Da.

The MPNs are constructed relying on coordination interaction between metal ions and catechol groups. The binding constant of the metal ion−ligand is an important parameter to study the complexation kinetics and structure, film stability, and environmental susceptibility. Herein, binding constants of ligand, that is catechol group in p(PEGMA-*co*-

DOI: 10.1021/acs.langmuir.9b01196
Langmuir 2019, 35, 8829−8839

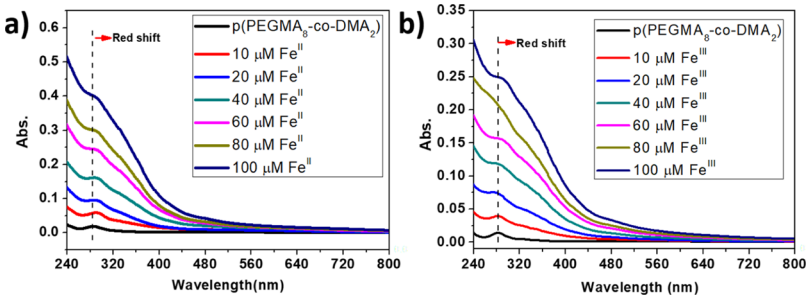

Figure 1. UV−vis spectroscopy measurements for the formation of the coordination structures between p(PEGMA$_8$-*co*-DMA$_2$) and metal ions of Fe^{II} (a) and Fe^{III} (b). The photometer was used with a scan range from 240 to 800 nm. The polymer solution was prepared at a concentration of 0.001% w/v in pH 8.5 Tris buffer and the Fe solution was mixed with the p(PEGMA-*co*-DMA) solution to attain a series of metal ion concentrations from 10 to 100 μM. The reaction proceeded at room temperature for 10 min before assessment.

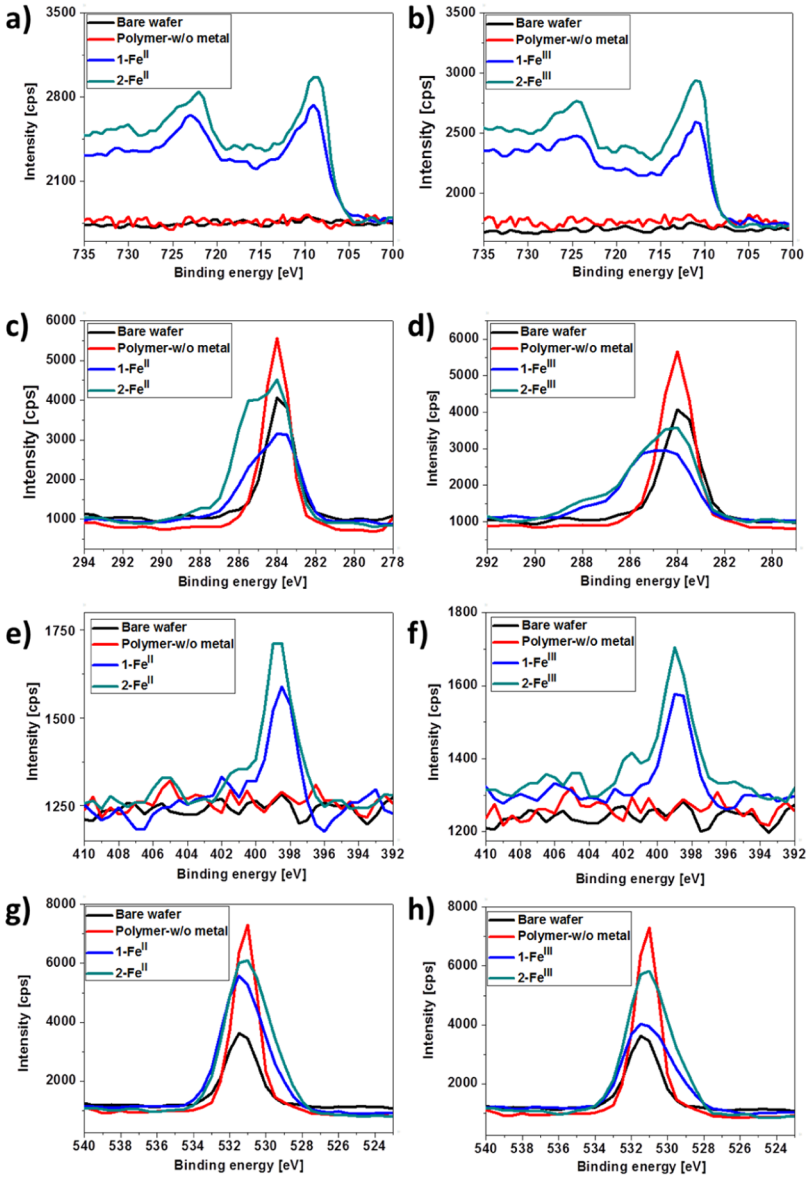

Figure 2. XPS spectra of Fe 2p (a,b), C 1s (c,d), N 1s (e,f), and O 1s (g,h) for MPN coatings of 1-Fe^{II}, 2-Fe^{II} (a,c,e,g), 1-Fe^{III} and 2-Fe^{III} (b,d,f,h), and reference samples of bare wafer and polymer film deposited without addition of metal ions.

DMA), and multivalent iron ions, that is Fe^{II} and Fe^{III}, were investigated using UV−vis spectroscopy as described in the Experimental Section. Evaluation of chelation properties of the catechol group was carried out by analyzing the absorbance and the shift of the peaks. In a solution containing p(PEGMA$_8$-*co*-DMA$_2$) alone, an absorbance peak centered at 288 nm was found, corresponding to the catechol group.[29,42,45,46] The intensity of the peak increased with the concentration of Fe^{II}

DOI: 10.1021/acs.langmuir.9b01196
Langmuir 2019, 35, 8829−8839

and Fe^{III}, and the peak red-shifted to a higher wavelength in the presence of iron ions, which related to the formation of complexation of iron ions and catechol groups (Figure 1). Moreover, new absorbance can be observed between 492 and 575 nm, indicating the formation of bis-complex and tri-complex structures between Fe ions and catechol groups in p(PEGMA$_8$-*co*-DMA$_2$) (Figure S2).[46] Moreover, the equilibrium binding constant, k, of iron ions with p(PEGMA$_8$-*co*-DMA$_2$) was estimated from the Klotz plots, based on the quantitative analysis of the absorbance of the samples at 288 nm (Figure S3). Thus, k values of Fe^{II}– and Fe^{III}–p(PEGMA$_8$-*co*-DMA$_2$) complexes were obtained to be 0.13 and 0.05 M^{-1}, respectively. The coordinative structure of Fe^{II}–p(PEGMA$_8$-*co*-DMA$_2$) provides a more stable coordination structure than Fe^{III}.

Cytotoxicity of p(PEGMA-*co*-DMA) Copolymers. A cytotoxicity test for the newly synthesized p(PEGMA-*co*-DMA) copolymers was essential for the development of a coating material in biomedical applications. The testing solutions containing p(PEGMA-*co*-DMA) at concentrations ranging from 0.2 to 25 mM were prepared in serum-free DMEM. The testing solutions were introduced to cell culture wells with NIH-3T3 fibroblasts for 24 h. The MTT assay was carried out for each sample and the viability of fibroblasts was calculated with respect to the cell sample without addition of copolymers. As shown in Figure S4, the cell viability remains above 80% for all concentrations of copolymers. Hydrophilic PEG is the major constitution of the copolymers and has proven its high biocompatibility for using in various medical applications.[47,48] The bioinspired DMA was derived from the natural DA, and has been applied for synthesis of underwater biocompatible adhesive[49,50] and medical coatings.[51] Therefore, the cytotoxicity induced by DMA-containing polymers was negligible. The results from the MTT assay confirm the biocompatibility of the copolymers for medical applications.

XPS Analysis for Surface Compositions. Chemical compositions of MPN coatings prepared from complexation of p(PEGMA$_8$-*co*-DMA$_2$) and iron ions with deposition cycle numbers of 1 and 2, that is samples of 1-Fe^{II}, 2-Fe^{II}, 1-Fe^{III}, and 2-Fe^{III}, on the substrates were characterized by XPS measurements in Figure 2 and Table 2. In addition, the reference samples, prepared on silicon wafers without modification and with deposition of p(PEGMA$_8$-*co*-DMA$_2$) alone (denoted as "polymer-w/o metal"), were included in the spectra for parallel comparison. The XPS spectra of Fe 2p (Figure 2a,b), C 1s (Figure 2c,d), N 1s (Figure 2e,f), and O 1s (Figure 2g,h) were recorded to determine the elemental compositions of the coatings. The spectra for the MPN coatings prepared from the mixture of p(PEGMA$_8$-*co*-DMA$_2$) and Fe^{II} are present on the left column of Figure 2a,c,e,g; that from the mixture of p(PEGMA$_8$-*co*-DMA$_2$) and Fe^{III} are shown on the right column of Figure 2b,d,f,h. In the spectra of Fe 2p, the spin orbital splitting doublet of metal oxide at BEs of 709.0 and 722.6 eV were observed, which correspond to Fe 2p$_{3/2}$ and Fe 2p$_{1/2}$ of Fe^{II}, respectively (Figure 2a).[52] A shoulder peak of Fe 2p$_{3/2}$ at 714.0 eV is assigned to be a satellite peak.[52] For the MPN films with Fe^{III} in Figure 3b, the relatively distinct peaks of Fe 2p$_{3/2}$ and Fe 2p$_{1/2}$ centered at BEs of 711.0 and 724.5 eV, respectively, were found. The spectra of Fe 2p indicate clearly the presence of iron ions in the MPN coatings. However, no peak in Fe 2p spectra was found from the reference samples. It should be noted that because the coatings were washed with copious deionized water to remove unbound substances, the peaks confirmed the presence of the chelated Fe ions within the polymer networks. In addition, the intensities of the peaks from samples of 2-Fe^{II} and 2-Fe^{III} are stronger than that of 1-Fe^{II} and 1-Fe^{III}, indicating the larger quantity of Fe ions in the films with the higher deposition number. From the analysis of C 1s spectra (Figure 2c,d), the peak components with BEs of 285.7 and 288 eV appearing in the MPN samples are associated with C–O and C=O species, respectively, indicating the presence of PEGMA.[53,54] The peak components with BE of 284.2 eV on bare wafer could be ascribed to the adventitious contamination of hydrocarbons from air.

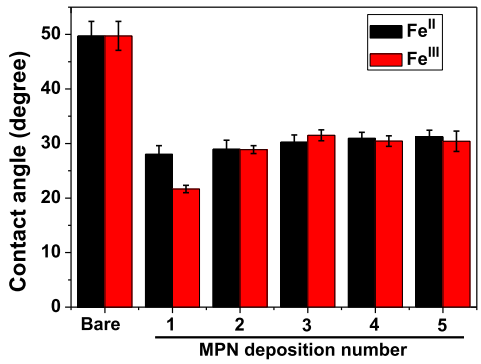

Figure 3. Contact angle measurements of MPN coatings with different deposition numbers. Triplicate tests were conducted.

Table 2. Atomic Concentration of MPN Coatings and Reference Samples Determined by XPS and Corrected by a Sensitivity Factor

	atomic percentage (%)				
sample	C	Fe	N	O	Si
wafer	28.81	0	0	44.45	26.74
polymer-w/o metal	48.96	0	0	29.51	21.53
1-Fe^{II}	48.55	3.21	2.87	37.24	8.13
2-Fe^{II}	51.64	3.54	3.32	32.94	5.53
1-Fe^{III}	47.99	2.38	2.13	37.16	10.34
2-Fe^{III}	50.27	3.49	2.76	36.61	6.87

The N 1s spectra for the coatings containing iron ions present peak components with a BE of 398.5 eV, which is associated with C–NH–CH in the DMA (Figure 2e,f). Nevertheless, no peak was found in the reference samples, revealing the absence of the copolymer on surfaces. As a result, the coordination-driven cross-linking and deposition for the film formation is proved.[28,29] Moreover, in the O 1s core-level spectra for the MPN coatings in Figure 2g,h, the peak components with BEs of 529.8, 532.2, 532.5, and 533.2 eV were observed, which contribute to FeO, O–C=O, C–O–C, and O–C=O, respectively.[53,54] Moreover, the HO–C in the catechol group can shift from 529 eV to a higher BE of 532 eV after chelation of iron ions because of the electron transfer from catechol to metal ions.[29] The deposition of copolymers through complexation of catechol–Fe was once again proved by the spectra of O 1s. In addition to the spectrum analysis, Table 2 presents the atomic concentrations of the MPN coatings and reference samples. The increase in the atomic percentages of Fe and N and decrease in that of Si with the deposition number indicated the growth of the MPN films. Therefore, the results from XPS spectra present three messages: (1) the deposition of copolymers on substrates was verified because of the presence of the backbone structures

DOI: 10.1021/acs.langmuir.9b01196
Langmuir 2019, 35, 8829–8839

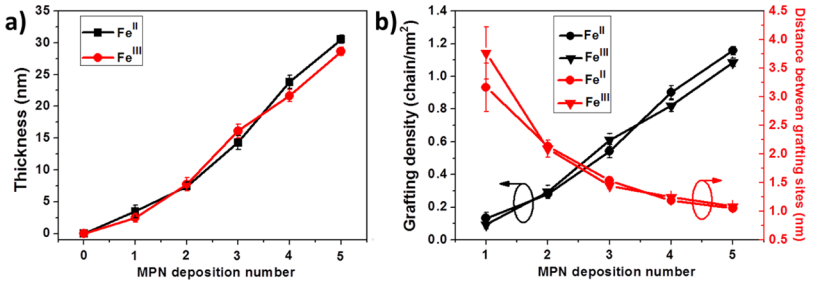

Figure 4. Thickness (a), grafting density, and distance between grafting sites (b); analysis of MPN after each deposition number (n = 3).

of acrylate and acrylamide as well as ether groups; (2) the coordination interaction between iron ions and catechol groups in copolymers was necessary for the deposition of the MPN films on surfaces; (3) the film thickness of the MPN coatings increases with the deposition number.

Surface Wettability of MPN Films on Substrates. The wettability of MPN films in terms of the deposition numbers was conducted using a contact angle goniometer. Bare glass substrates with a water static contact angle of $\theta = 49.7 \pm 2.6°$ are found in Figure 3. The MPN films were prepared on the O_2 plasma-treated glass substrates by co-deposition of p(PEGMA$_8$-*co*-DMA$_2$) with either Fe^{II} or Fe^{III} with various deposition numbers from 1 to 5, that is samples of *n*-Fe^{II} and *n*-Fe^{III}, where *n* is 1 to 5. The contact angles of samples slightly increased with the deposition number and eventually reached around $\theta = 30°$. The plasma-treated glass is superhydrophilic with a contact angle of $\theta < 5°$. As a result, the presence of PEG on surfaces can lead to higher contact angles, reflecting the amphiphilic character of PEG.[55] Nevertheless, the surface wettability of MPN coatings became steady after the multiple deposition.

Ellipsometric Analysis of MPN Coatings. The thickness of MPN coatings prepared by co-deposition of p(PEGMA$_8$-*co*-DMA$_2$) with either Fe^{II} or Fe^{III} with a deposition number from 1 to 5 on wafers was measured using ellipsometry. As shown in Figure 4, the thicknesses of MPN coatings increased with the deposition number, and reached d = 30.5 and 28.6 nm for 5-Fe^{II} and 5-Fe^{III}, respectively. In addition, the MPN films coordinated with Fe^{II} or Fe^{III} exhibited comparable film thicknesses on the same basis of the deposition number. According to the hard−soft acid base theory, the phenolic ligand serves as hard Lewis base, leading to the large metal-binding constant with hard Lewis acid, such as Fe^{III}.[56] Moreover, Fe^{II} is a moderate Lewis acid, which is expected to have a weaker interaction with DMA. For example, the binding constants of polyphenolic tannic acid is $k = 10^4$ M^{-4}, and 10^{17} M^{-4} with Fe^{II} and Fe^{III}, respectively.[57−59] Interestingly, k values of Fe^{II}− and Fe^{III}−p(PEGMA$_8$-*co*-DMA$_2$) complexes were obtained to be 0.13 and 0.05 M^{-1}, respectively, in this work. However, the interactions between the catecholic group on DMA and iron metals did not show an obvious difference in terms of the film thickness, which may be ascribed to change in acidity of the catecholic group and oxidation of Fe^{II}.

The grafting density, Σ, and distance between grafting site, D, were estimated from the data of M_n and film thickness with an attempt to compare with polymer brushes prepared by surface-initiated polymerization.[43] Unlike the polymer brushes, the grafting density of which was determined by initiator surface density and polymerization conditions, the MPN coatings, prepared by the grafting-onto approach, allow varying the grafting density and distance between grafting sites by controlling the deposition number. As shown in Figure 4b, the grafting density increased with the deposition numbers, which approximately changed from 0.1 to 1.1 chains nm^{-2} when the deposition numbers increased from 1 to 5. For the MPN films with higher deposition numbers, the grafting density is comparable with that obtained from surface-initiated polymerization (∼0.7 chains nm^{-2}).[43] Additionally, the distance between grafting sites decreased with the increase in the deposition number, reflecting increased occupation of polymers on a unit area. It should be noted that the MPN films are a three-dimensional network structure, other than the two-dimensional polymer brushes. Therefore, the gyration of polymer chains in the MPN films should be the same under the identical deposition environment. The high grafting density and short distance between grafting sites should be explained by the high surface concentration from the top view, instead of the crowdedness of polymer chains as found in polymer brushes. Nevertheless, the surface properties of the substrates should be determined by the coatings that enable shielding the surfaces and providing the excluded volume.

Surface Topological Analysis of MPN Films. AFM was used to further characterize surface morphology of MPN samples of 3-Fe^{II} and 3-Fe^{III} with p(PEGMA$_8$-*co*-DMA$_2$) in comparison with bare silicon wafer in Figure S5. The average roughness (R_a) of the bare sample is 0.5 ± 0.2 nm, whereas the R_a values of the 3-Fe^{II} and 3-Fe^{III} increased to 58.3 ± 3.2 and 55.9 ± 1.2 nm, respectively. Evidently, the MPN films displayed a higher roughness and exhibited large amounts of aggregates deposited on surfaces. The aggregates should be attributed to the complexation of catechol groups in polymer chains with metal ions. It is suspected that the aggregates should form in the coating solution and then deposit onto the substrates. Previous work indicated that catecholic molecule is mobile at the high ligand concentration and can form tris-type complexes locally or as a whole with metal ions in a solution.[60] Therefore, the roughness of the coatings can be reduced by controlling the concentration of the polymers and metal ions, leading to less aggregation in solutions.

Stability Test of MPN on Substrates. The formation of MPN films was based on the coordination bonds between metal ions and catechol moieties, which is a pH-sensitive interaction.[27,28] Thus, evaluation of the network stability was conducted by observing the change in the thickness of the biomimetic MPN films as a function of time under different pH conditions. The 3-Fe^{II} coating on silicon wafers was submerged in buffered solutions at pH of 5, 7.4, and 10. An ellipsometer was employed to follow the thickness changes. As indicated in Figure 5, the thickness of the 3-Fe^{II} films in an acidic solution dropped more rapidly than that in neutral and alkaline solutions, which is in agreement with previous works.[27,28] After incubation for 20 h, the thickness of the MPN films on surfaces in the solution at pH 5 considerably reduced by 82%, whereas that at pH 7.4 decreased by only 22%. As a result, the MPN films possessed

DOI: 10.1021/acs.langmuir.9b01196
Langmuir 2019, 35, 8829−8839

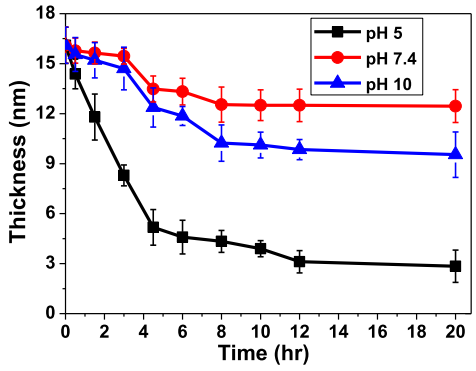

Figure 5. Time revolution of ellipsometric thickness of the MPN sample of 3-Fe^{II} in solutions at different pH values.

good stability in a physiological environment, but in an acidic environment, such as tumor microenvironment and lysosome, the MPN structure will disassemble by breaking the coordination interaction. Consequently, the pegylated MPN structure will be particularly interesting in drug delivery and design for smart materials.

Antifouling Properties of Pegylated MPN Films. Hydrophilic PEG has been well known as a biocompatible and antifouling material for a wide spectrum of applications in the medical field.[12−14] Herein, surface pegylation was conducted by the formation of p($PEGMA_8$-*co*-DMA_2) MPN films through coupling with Fe^{II} and Fe^{III} for fouling resistance against NIH-3T3 fibroblasts and bacteria. The coatings with different deposition numbers were prepared on glass substrates and the adhesions of cells and bacteria were microscopically observed and counted using ImageJ software. In Figure 6a, the cell adhesion assay with NIH-3T3 fibroblasts shows that the pegylated surfaces with the MPN coatings enable resisting cell adsorption to a relatively low level with respect to that on bare glass substrates. The adherent cell numbers were inversely proportional to the deposition numbers of the MPN coatings. Moreover, the MPN−Fe^{II} coatings show better fouling resistance than the MPN−Fe^{III} coatings on the same basis of the deposition number, which can be ascribed to the stable coordinative properties of Fe^{II} with p(PEGMA-*co*-DMA).

Gram-positive and Gram-negative bacteria of *E. coli* and *S. epidermidis*, respectively, were chosen for the fouling tests on the bare glass and MPN coatings. The samples were immersed into bacterial solutions, and the presence and viability of adherent bacteria were probed by using a Live/Dead staining kit (Figure S6). As present in Figures 6b and S7 for *E. coli* and *S. epidermidis*, respectively, considerable suppression in bacterial adhesion was found on the MPN-coated substrates compared with that on bare glass. The biofouling tests with fibroblasts and bacteria reflect the fact that the surface pegylation by deposition of p($PEGMA_8$-*co*-DMA_2) offers high hydrophilicity, large excluded volume, lack of protein binding sites, high molecular mobility, and osmotic repulsion to effectively expel the nonspecific adsorption.[61,62] Interestingly, comparable antifouling capabilities for fibroblasts and bacteria were found for the MPN coatings with different polymer compositions, that is p($PEGMA_7$-*co*-DMA_3) and p($PEGMA_9$-*co*-DMA_1), as demonstrated in Figure S8. In addition, the fraction dead on the MPN coatings generally increased with the deposition numbers, which is most likely due to the metal ion releasing from the MPN networks. Many reports have shown that toxic doses of certain metal ions increase intracellular ROS.[63−68] Fe-catalyzed autoxidation initiates the production of reduced forms of molecular oxygen (O_2), such as H_2O_2 and $O_2^{\bullet-}$.[63] The process is driven by the Fenton reaction.[63,69] The radicals interfere in cell membrane formation of bacteria, and cause organelle damage and gene mutation, leading to death of the adsorbed bacteria.[70,71] Moreover, the redox cycling of metals might consume cellular antioxidants. Therefore, metal ions can effectively exert antimicrobial activity.

Universal MPN Coatings on Different Types of Substrates. The MPN coatings of 2-Fe^{II} and 2-Fe^{III} were prepared on various substrates of glass (SiO_2), Nitinol (Ni−Ti alloy), PDMS, PS, silicon wafer, and TiO_2, which are raw materials regularly used in medical applications. The fouling tests with *E. coli* for bare and MPN-modified samples were carried out and compared with corresponding bare substrates as indicated in Figure 7. Obviously, the MPN coatings enable suppressing bacterial adhesion regardless of the underlying substrates. From the quantitative analysis, the reduction rates of bacteria on MPN coatings reach 90%. The substrate-independent deposition of MPN coatings using natural polyphenol tannic acid (TA) and Fe^{III} ions was demonstrated.[29] In this work, synthetic catechol-containing antifouling polymers were deposited onto a wide range of materials by the formation of a complex structure with metal ions for potential exploitation in a wide spectrum of medical devices for antifouling properties.

CONCLUSIONS

In this work, catechol-containing p(PEGMA-*co*-DMA) polymers were synthesized as molecular building blocks, and deposited on substrates by reacting with metal ions of Fe^{II} and Fe^{III} to form cross-linked films. The formation and interfacial

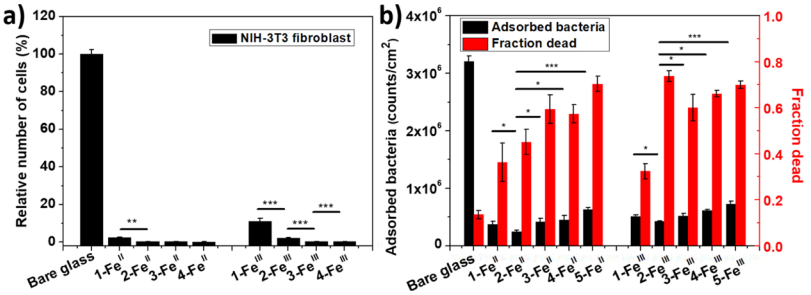

Figure 6. (a) Relative numbers of NIH-3T3 fibroblasts on MPN coatings with respect to bare glass. The MPN coatings were prepared by co-deposition of p($PEGMA_8$-*co*-DMA_2) and metal ions of Fe^{II} or Fe^{III} with different deposition numbers. (b) Total number of adsorbed bacteria counts per area (black bars) and fraction of bacteria dead (red bars) for *E. coli* on bare glass and MPN-coated substrates. Values in (a,b) represent the mean and the standard deviation (n = 3). *, **, *** represent $p < 0.05$, $p < 0.01$, $p < 0.001$, respectively.

DOI: 10.1021/acs.langmuir.9b01196
Langmuir 2019, 35, 8829−8839

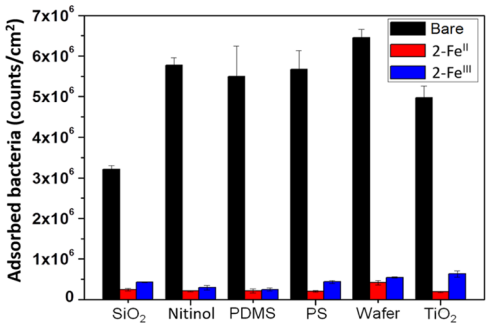

Figure 7. Total number of adsorbed bacterial counts per area on various types of substrates with and without MPN coatings of 2-Fe^{II} and 2-Fe^{III}. The fouling tests were conducted with *E. coli*. Values represent the mean and the standard deviation (n = 3).

properties were characterized by using UV−vis spectroscopy, contact angle goniometer, XPS, ellipsometry, and AFM. The thickness, grafting density, coverage, and roughness of the MPN coatings increased with the deposition number. The calculation for equilibrium binding constants reveals that the MPN coatings with Fe^{II} provides better stability than that with Fe^{III}. Moreover, the pH responsive property of the MPN coatings was accessed, showing a quick disassembly of the networks at low pH. Good biocompatibility of the polymers ensures the potential medical applications. Herein, the antifouling and antimicrobial properties of the MPN coatings were demonstrated on various types of substrates. Thus, we can envision that the present study represents a promising strategy to provide an important insight into the synthetic MPN-assisted approach, thereby paving the way for major benefits to medical coatings.

■ ASSOCIATED CONTENT

Supporting Information

The Supporting Information is available free of charge on the ACS Publications website at DOI: 10.1021/acs.langmuir.9b01196.

^{1}H NMR spectrum of DMA; UV−vis spectroscopy measurements for the formation of the coordination structures between p($PEGMA_8$-co-DMA_2) and metal ions of Fe^{II} and FE^{III}; Klotz plots for binding constant of Fe^{II} and Fe^{III} with p($PEGMA_8$-co-DMA_2); cell viability of 3T3 fibroblasts for examining the cytotoxicity of p(PEGMA-co-DMA) in a range of concentrations in serum-free culture medium; AFM topography images of bare, 3-Fe^{II}, and 3-Fe^{III}; fluorescence images of live and dead *E. coli* on samples; total number of absorbed bacteria counts per area and fraction of bacteria dead for *S. epidermidis* on bare glass and MPN-coated substrates; and relative number of NIH-3T3 fibroblasts on MPN coatings with respect to bare glass and total number of absorbed bacteria counts per area for *E. coli* on bare and MPN-coated substrates (PDF)

■ AUTHOR INFORMATION

Corresponding Authors

*E-mail: wangyi@wibe.ac.cn (Y.W.).
*E-mail: cjhuang@ncu.edu.tw (C.-J.H.).

ORCID

Chun-Jen Huang: 0000-0001-9832-5812

Notes

The authors declare no competing financial interest.

■ ACKNOWLEDGMENTS

The authors acknowledge the Ministry of Science and Technology (MOST 105-2628-E-008-007-MY3) for financial support of this project.

■ REFERENCES

(1) Smeltzer, M. S.; Nelson, C. L.; Evans, R. P. Biofilms and aseptic loosening. *The Role of Biofilms in Device-Related Infections*; Springer, 2008; pp 57−74.
(2) Banerjee, I.; Pangule, R. C.; Kane, R. S. Antifouling coatings: recent developments in the design of surfaces that prevent fouling by proteins, bacteria, and marine organisms. *Adv. Mater.* **2011**, *23*, 690−718.
(3) Yeh, P.-Y. J.; Kizhakkedathu, J. N.; Madden, J. D.; Chiao, M. Electric field and vibration-assisted nanomolecule desorption and anti-biofouling for biosensor applications. *Colloids Surf., B* **2007**, *59*, 67−73.
(4) Dobretsov, S. Expected effect of climate change on fouling communities and its impact on antifouling research. *Advances in Marine Antifouling Coatings and Technologies*; Elsevier, 2009; pp 222−239.
(5) Pangarkar, B. L.; Sane, M. G.; Guddad, M. Reverse osmosis and membrane distillation for desalination of groundwater: a review. *ISRN Mater. Sci.* **2011**, *2011*, 523124.
(6) Lebret, K.; Thabard, M.; Hellio, C. Algae as marine fouling organisms: adhesion damage and prevention. *Advances in Marine Antifouling Coatings and Technologies*; Elsevier, 2009; pp 80−112.
(7) Railkin, A. I. *Marine Biofouling: Colonization Processes and Defenses*; CRC press, 2003.
(8) Vo-Dinh, T. *Nanotechnology in Biology and Medicine: Methods, Devices, and Applications*; CRC Press, 2007.
(9) Mah, T.-F. C.; O'Toole, G. A. Mechanism of biofilm resistance to antimicrobial agents. *Trends Microbiol.* **2001**, *9*, 34−39.
(10) Stoodley, P.; Sauer, K.; Davies, D. G.; Costerton, J. W. Biofilms as complex differentiated communities. *Annu. Rev. Microbiol.* **2002**, *56*, 187−209.
(11) Banerjee, I.; Pangule, R. C.; Kane, R. S. Antifouling coatings: recent developments in the design of surfaces that prevent fouling by proteins, bacteria, and marine organisms. *Adv. Mater.* **2011**, *23*, 690−718.
(12) Rundqvist, J.; Hoh, J. H.; Haviland, D. B. Poly(ethylene glycol) Self-Assembled Monolayer Island Growth. *Langmuir* **2005**, *21*, 2981−2987.
(13) Zoulalian, V.; Monge, S.; Zürcher, S.; Textor, M.; Robin, J. J.; Tosatti, S. Functionalization of Titanium Oxide Surfaces by Means of Poly(alkyl-phosphonates). *J. Phys. Chem. B* **2006**, *110*, 25603−25605.
(14) Kohler, N.; Fryxell, G. E.; Zhang, M. A Bifunctional Poly(ethylene glycol) Silane Immobilized on Metallic Oxide-Based Nanoparticles for Conjugation with Cell Targeting Agents. *J. Am. Chem. Soc.* **2004**, *126*, 7206−7211.
(15) Francolini, I.; Silvestro, I.; Di Lisio, V.; Martinelli, A.; Piozzi, A. Synthesis, Characterization, and Bacterial Fouling-Resistance Properties of Polyethylene Glycol-Grafted Polyurethane Elastomers. *Int. J. Mol. Sci.* **2019**, *20*, 1001.
(16) Yuan, P.; Qiu, X.; Wang, X.; Tian, R.; Wang, L.; Bai, Y.; Liu, S.; Chen, X. Substrate-Independent Coating with Persistent and Stable Antifouling and Antibacterial Activities to Reduce Bacterial Infection for Various Implants. *Adv. Healthcare Mater.* **2019**, *8*, 1801423.
(17) Su, X.; Hao, D.; Li, Z.; Guo, X.; Jiang, L. Design of hierarchical comb hydrophilic polymer brush (HCHPB) surfaces inspired by fish mucus for anti-biofouling. *J. Mater. Chem. B* **2019**, *7*, 1322−1332.
(18) Luk, Y.-Y.; Kato, M.; Mrksich, M. Self-assembled monolayers of alkanethiolates presenting mannitol groups are inert to protein adsorption and cell attachment. *Langmuir* **2000**, *16*, 9604−9608.
(19) Ostuni, E.; Chapman, R. G.; Holmlin, R. E.; Takayama, S.; Whitesides, G. M. A survey of structure− property relationships of

DOI: 10.1021/acs.langmuir.9b01196
Langmuir 2019, 35, 8829−8839

surfaces that resist the adsorption of protein. *Langmuir* **2001**, *17*, 5605−5620.
(20) Leckband, D.; Sheth, S.; Halperin, A. Grafted poly (ethylene oxide) brushes as nonfouling surface coatings. *J. Biomater. Sci., Polym. Ed.* **1999**, *10*, 1125−1147.
(21) Jiang, S.; Cao, Z. Ultralow-fouling, functionalizable, and hydrolyzable zwitterionic materials and their derivatives for biological applications. *Adv. Mater.* **2010**, *22*, 920−932.
(22) Perikamana, S. K. M.; Lee, J.; Lee, Y. B.; Shin, Y. M.; Lee, E. J.; Mikos, A. G.; Shin, H. Materials from Mussel-Inspired Chemistry for Cell and Tissue Engineering Applications. *Biomacromolecules* **2015**, *16*, 2541−2555.
(23) Kwon, I. S.; Bettinger, C. J. Polydopamine nanostructures as biomaterials for medical applications. *J. Mater. Chem. B* **2018**, *6*, 6895−6903.
(24) Lee, H.; Dellatore, S. M.; Miller, W. M.; Messersmith, P. B. Mussel-inspired surface chemistry for multifunctional coatings. *Science* **2007**, *318*, 426−430.
(25) Harrington, M. J.; Masic, A.; Holten-Andersen, N.; Waite, J. H.; Fratzl, P. Iron-Clad Fibers: A Metal-Based Biological Strategy for Hard Flexible Coatings. *Science* **2010**, *328*, 216−220.
(26) Holten-Andersen, N.; Fantner, G. E.; Hohlbauch, S.; Waite, J. H.; Zok, F. W. Protective coatings on extensible biofibres. *Nat. Mater.* **2007**, *6*, 669−672.
(27) Guo, J.; Ping, Y.; Ejima, H.; Alt, K.; Meissner, M.; Richardson, J. J.; Yan, Y.; Peter, K.; von Elverfeldt, D.; Hagemeyer, C. E.; Caruso, F. Engineering Multifunctional Capsules through the Assembly of Metal-Phenolic Networks. *Angew. Chem., Int. Ed.* **2014**, *53*, 5546−5551.
(28) Ejima, H.; Richardson, J. J.; Caruso, F. Metal-phenolic networks as a versatile platform to engineer nanomaterials and biointerfaces. *Nano Today* **2017**, *12*, 136−148.
(29) Ejima, H.; Richardson, J. J.; Liang, K.; Best, J. P.; van Koeverden, M. P.; Such, G. K.; Cui, J.; Caruso, F. One-step assembly of coordination complexes for versatile film and particle engineering. *Science* **2013**, *341*, 154−157.
(30) Xu, Z. Mechanics of metal-catecholate complexes: The roles of coordination state and metal types. *Sci. Rep.* **2013**, *3*, 2914.
(31) Richardson, J. J.; Cui, J.; Björnmalm, M.; Braunger, J. A.; Ejima, H.; Caruso, F. Innovation in Layer-by-Layer Assembly. *Chem. Rev.* **2016**, *116*, 14828−14867.
(32) Rahim, M. A.; Björnmalm, M.; Suma, T.; Faria, M.; Ju, Y.; Kempe, K.; Müllner, M.; Ejima, H.; Stickland, A. D.; Caruso, F. Metal-Phenolic Supramolecular Gelation. *Angew. Chem., Int. Ed.* **2016**, *55*, 13803−13807.
(33) Liang, G.; Xu, J.; Wang, X. Synthesis and characterization of organometallic coordination polymer nanoshells of prussian blue using miniemulsion periphery polymerization (MEPP). *J. Am. Chem. Soc.* **2009**, *131*, 5378−5379.
(34) Roy, X.; Hui, J. K.-H.; Rabnawaz, M.; Liu, G.; MacLachlan, M. J. Prussian Blue Nanocontainers: Selectively Permeable Hollow Metal−Organic Capsules from Block Ionomer Emulsion-Induced Assembly. *J. Am. Chem. Soc.* **2011**, *133*, 8420−8423.
(35) Shi, J.; Zhang, L.; Jiang, Z. Facile construction of multicompartment multienzyme system through layer-by-layer self-assembly and biomimetic mineralization. *ACS Appl. Mater. Interfaces* **2011**, *3*, 881−889.
(36) Holten-Andersen, N.; Harrington, M. J.; Birkedal, H.; Lee, B. P.; Messersmith, P. B.; Lee, K. Y. C.; Waite, J. H. pH-induced metal-ligand cross-links inspired by mussel yield self-healing polymer networks with near-covalent elastic moduli. *Proc. Natl. Acad. Sci. U.S.A.* **2011**, *108*, 2651−2655.
(37) Ju, Y.; Cui, J.; Müllner, M.; Suma, T.; Hu, M.; Caruso, F. Engineering Low-Fouling and pH-Degradable Capsules through the Assembly of Metal-Phenolic Networks. *Biomacromolecules* **2015**, *16*, 807−814.
(38) Kim, S.; Gim, T.; Jeong, Y.; Ryu, J. H.; Kang, S. M. Facile Construction of Robust Multilayered PEG Films on Polydopamine-Coated Solid Substrates for Marine Antifouling Applications. *ACS Appl. Mater. Interfaces* **2018**, *10*, 7626−7631.
(39) Park, J. H.; Kim, K.; Lee, J.; Choi, J. Y.; Hong, D.; Yang, S. H.; Caruso, F.; Lee, Y.; Choi, I. S. A Cytoprotective and Degradable Metal-Polyphenol Nanoshell for Single-Cell Encapsulation. *Angew. Chem., Int. Ed.* **2014**, *53*, 12420.
(40) Lemire, J. A.; Harrison, J. J.; Turner, R. J. Antimicrobial activity of metals: mechanisms, molecular targets and applications. *Nat. Rev. Microbiol.* **2013**, *11*, 371−384.
(41) Xu, L. Q.; Pranantyo, D.; Ng, Y. X.; Teo, S. L.-M.; Neoh, K.-G.; Kang, E.-T.; Fu, G. D. Antifouling Coatings of Catecholamine Copolymers on Stainless Steel. *Ind. Eng. Chem. Res.* **2015**, *54*, 5959−5967.
(42) Kolaylı, S.; Ocak, M.; Küçük, M.; Abbasoğlu, R. Does caffeine bind to metal ions? *Food Chem.* **2004**, *84*, 383−388.
(43) Melzak, K. A.; Yu, K.; Bo, D.; Kizhakkedathu, J. N.; Toca-Herrera, J. L. Chain Length and Grafting Density Dependent Enhancement in the Hydrolysis of Ester-Linked Polymer Brushes. *Langmuir* **2015**, *31*, 6463−6470.
(44) Luzinov, I.; Julthongpiput, D.; Malz, H.; Pionteck, J.; Tsukruk, V. V. Polystyrene Layers Grafted to Epoxy-Modified Silicon Surfaces. *Macromolecules* **2000**, *33*, 1043−1048.
(45) Guo, J.; Ping, Y.; Ejima, H.; Alt, K.; Meissner, M.; Richardson, J. J.; Yan, Y.; Peter, K.; von Elverfeldt, D.; Hagemeyer, C. E.; Caruso, F. Engineering multifunctional capsules through the assembly of metal-phenolic networks. *Angew. Chem., Int. Ed.* **2014**, *53*, 5546−5551.
(46) Ju, Y.; Cui, J.; Müllner, M.; Suma, T.; Hu, M.; Caruso, F. Engineering low-fouling and pH-degradable capsules through the assembly of metal-phenolic networks. *Biomacromolecules* **2015**, *16*, 807−814.
(47) Alcantar, N. A.; Aydil, E. S.; Israelachvili, J. N. Polyethylene glycol-coated biocompatible surfaces. *J. Biomed. Mater. Res.* **2000**, *51*, 343−351.
(48) Knop, K.; Hoogenboom, R.; Fischer, D.; Schubert, U. S. Poly(ethylene glycol) in drug delivery: pros and cons as well as potential alternatives. *Angew. Chem., Int. Ed. Engl.* **2010**, *49*, 6288−6308.
(49) Glass, P.; Chung, H.; Washburn, N. R.; Sitti, M. Enhanced Reversible Adhesion of Dopamine Methacrylamide-Coated Elastomer Microfibrillar Structures under Wet Conditions. *Langmuir* **2009**, *25*, 6607−6612.
(50) Chung, H.; Glass, P.; Pothen, J. M.; Sitti, M.; Washburn, N. R. Enhanced Adhesion of Dopamine Methacrylamide Elastomers via Viscoelasticity Tuning. *Biomacromolecules* **2011**, *12*, 342−347.
(51) Wang, B. L.; Jin, T. W.; Han, Y. M.; Shen, C. H.; Li, Q.; Lin, Q. K.; Chen, H. Bio-inspired terpolymers containing dopamine, cations and MPC: a versatile platform to construct a recycle antibacterial and antifouling surface. *J. Mater. Chem. B* **2015**, *3*, 5501−5510.
(52) Yamashita, T.; Hayes, P. Analysis of XPS spectra of Fe2+ and Fe3+ ions in oxide materials. *Appl. Surf. Sci.* **2008**, *254*, 2441−2449.
(53) McIntyre, N. S.; Zetaruk, D. G. X-ray photoelectron spectroscopic studies of iron oxides. *Anal. Chem.* **1977**, *49*, 1521−1529.
(54) Liu, C.-Y.; Huang, C.-J. Functionalization of Polydopamine via the Aza-Michael Reaction for Antimicrobial Interfaces. *Langmuir* **2016**, *32*, 5019−5028.
(55) Yuan, S.; Wan, D.; Liang, B.; Pehkonen, S. O.; Ting, Y. P.; Neoh, K. G.; Kang, E. T. Lysozyme-coupled poly (poly (ethylene glycol) methacrylate)− stainless steel hybrids and their antifouling and antibacterial surfaces. *Langmuir* **2011**, *27*, 2761−2774.
(56) Pearson, R. G. Hard and Soft Acids and Bases. *J. Am. Chem. Soc.* **1963**, *85*, 3533−3539.
(57) Theis, T. L.; Singer, P. C. Complexation of iron(II) by organic matter and its effect on iron(II) oxygenation. *Environ. Sci. Technol.* **1974**, *8*, 569−573.
(58) Iffat, A. T.; Maqsood, Z. T.; Ali, K.; Nisar, S. Interaction of tannic acid with higher oxidation state of iron. *J. Chem. Soc. Pak.* **2004**, *26*, 151−156.
(59) Sungur, Ş.; Uzar, A. Investigation of complexes tannic acid and myricetin with Fe(III). *Spectrochim. Acta, Part A* **2008**, *69*, 225−229.
(60) Rahim, M. A.; Ejima, H.; Cho, K. L.; Kempe, K.; Müllner, M.; Best, J. P.; Caruso, F. Coordination-Driven Multistep Assembly of

DOI: 10.1021/acs.langmuir.9b01196
Langmuir 2019, 35, 8829−8839

Metal-Polyphenol Films and Capsules. *Chem. Mater.* **2014**, *26*, 1645−1653.
(61) Gombotz, W. R.; Guanghui, W.; Horbett, T. A.; Hoffman, A. S. PROTEIN ADSORPTION TO POLY(ETHYLENE OXIDE) SURFACES. *J. Biomed. Mater. Res.* **1991**, *25*, 1547−1562.
(62) Ostuni, E.; Chapman, R. G.; Holmlin, R. E.; Takayama, S.; Whitesides, G. M. A survey of structure-property relationships of surfaces that resist the adsorption of protein. *Langmuir* **2001**, *17*, 5605−5620.
(63) Valko, M.; Morris, H.; Cronin, M. Metals, toxicity and oxidative stress. *Curr. Med. Chem.* **2005**, *12*, 1161−1208.
(64) Macomber, L.; Rensing, C.; Imlay, J. A. Intracellular copper does not catalyze the formation of oxidative DNA damage in Escherichia coli. *J. Bacteriol.* **2007**, *189*, 1616−1626.
(65) Harrison, J. J.; Tremaroli, V.; Stan, M. A.; Chan, C. S.; Vacchi-Suzzi, C.; Heyne, B. J.; Parsek, M. R.; Ceri, H.; Turner, R. J. Chromosomal antioxidant genes have metal ion-specific roles as determinants of bacterial metal tolerance. *Environ. Microbiol.* **2009**, *11*, 2491−2509.
(66) Nunoshiba, T.; Obata, F.; Boss, A. C.; Oikawa, S.; Mori, T.; Kawanishi, S.; Yamamoto, K. Role of iron and superoxide for generation of hydroxyl radical, oxidative DNA lesions, and mutagenesis in Escherichia coli. *J. Biol. Chem.* **1999**, *274*, 34832−34837.
(67) Santo, C. E.; Lam, E. W.; Elowsky, C. G.; Quaranta, D.; Domaille, D. W.; Chang, C. J.; Grass, G. Bacterial Killing by Dry Metallic Copper Surfaces. *Appl. Environ. Microbiol.* **2011**, *77*, 794−802.
(68) Warnes, S. L.; Caves, V.; Keevil, C. W. Mechanism of copper surface toxicity in Escherichia coli O157:H7 and Salmonella involves immediate membrane depolarization followed by slower rate of DNA destruction which differs from that observed for Gram-positive bacteria. *Environ. Microbiol.* **2012**, *14*, 1730−1743.
(69) Stohs, S.; Bagchi, D. Oxidative mechanisms in the toxicity of metal ions. *Free Radicals Biol. Med.* **1995**, *18*, 321−336.
(70) Lemire, J. A.; Harrison, J. J.; Turner, R. J. Antimicrobial activity of metals: mechanisms, molecular targets and applications. *Nat. Rev. Microbiol.* **2013**, *11*, 371−384.
(71) Cortes-Cortes, P.; ATRIA, A.; Contreras, M.; Peña, O.; Fernández, K.; Corsini, G. Magnetic behavior and antibacterial activity of iron (III) complexes. *J. Chil. Chem. Soc.* **2008**, *53*, 1527−1532.

DOI: 10.1021/acs.langmuir.9b01196
Langmuir 2019, 35, 8829−8839